TUM

TECHNISCHE UNIVERSITÄT MÜNCHEN
INSTITUT FÜR INFORMATIK

MultiIMU: Fusing Multiple Calibrated IMUs For Enhanced Mixed Reality Tracking

Adnane Jadid, Linda Rudolph, Frieder Pankratz, Kai Wu, Pengyuan Wang and Gudrun Klinker

TUM-I1976

MultiIMU:fusing Multiple Calibrated IMUs for Enhanced Mixed Reality Tracking

Adnane Jadid*
Technical University of Munich
Linda Rudolph†
Technical University of Munich
Frieder Pankratz‡
Technical University of Munich
Kai Wu§
Technical University of Munich
Pengyuan Wang¶
Technical University of Munich
Gudrun Klinker‖
Technical University of Munich

ABSTRACT

Low-cost mobile mixed reality solutions for head tracking, as well as tracking of interaction targets, can be enhanced by multiple inertial measurement units (IMUs). Since microelectro-mechanical systems (MEMS) were introduced, IMUs have become smaller, they need less power and cost less. Yet, as any sensor, IMUs produce sensor error and mitigate the accuracy of the tracking system. This is particularly the case for low-cost IMUs. In this article, we investigate whether the joint use of three IMUs can reduce the overall error. We present a solution fusing three independently calibrated low-cost IMUs on a planar and non-planar grid. We show that we can achieve the tracking quality of a single high-cost IMU this way. For the comparison, we offer several one Degree of Freedom measurement setups for mechanical rotation and translation movements. Afterwards, we discuss some concepts towards designing non-planar arrangements of Multi-IMUs in a Grid that may be suitable for HMD tracking.

Index Terms: Inertial Tracking—Sensor Fusion—calibration—Registration—-Error Modelling

1 INTRODUCTION

An IMU is an electronic device that senses the change of kinematic energy of a moving body. IMUs are often incorporated in navigation systems. The insensitivity to occlusions and illuminations make them a good complement for other tracking modalities such as optical. Apart from navigation purposes, IMUs are also used in applications including robotics, head-mounted devices (HMD) for virtual reality, remote gaming controllers, and the balancing system of Segways.

Typical configurations of an IMU are composed of three accelerometers, three gyroscopes and sometimes also a magnetometer for the three Cartesian axes. An IMU works by detecting the current rate of acceleration, as well as changes in rotational attributes, including pitch, roll and yaw [5].

The accuracy of an IMU depends on a variety of errors and on the effectiveness of the updating procedure in reducing these errors. High quality IMUs provide an onboard calibration and accurate results. Yet, they cost about the same or more than AR/VR-related mobile devices and are thus too expensive to be included in Smartphones or HMDs. For such AR-related application scenarios, we are investigating low-cost multi-IMU setups. We expect such cheap multi-IMU based tracking to be also suitable for tangible gadgets in AR and VR applications. Instead, low-cost IMUs with low two digit prices are used despite their disadvantage of lower quality.

This article focuses on low-cost multi-IMU setups, investigating whether several low-cost IMUs together can achieve similar performance as a single high-cost IMU. To this end, we investigate the impact of calibration as well as various sensor fusion concepts on the achievable accuracy. We compare the accuracy of a high-cost IMU with a number of low-cost variants: a) with a single calibrated low-cost IMU, b) with multi-registered fused low-cost IMUs and c) with multi calibrated registered fused low-cost IMUs. We use a linear slider and a rotation platform as 1-DoF measurement setups to systematically investigate rotational and translational movements. These known mechanical movements can be employed as ground truth and for the definition of a motion model. We apply a root mean square error (RMSE) comparison analysis to evaluate the accuracy.

Combined use of multiple low-cost IMUs can improve the quality of mixed reality tracking. Several approaches have been already been proposed to achieve better performance and high accuracy. Shahri and Rasoulzadeh have presented a homogenous multi-sensor fusion technique to evaluate the true angular rate and acceleration with a combination of four low-cost IMUs based on the Steady State Kalman Filter [14]. Skog et al. [15] implemented a low-cost multi inertial measurement unit (MIMU) systems platform. Further, Bancroft and Lachapelle [3] developed several fusion algorithms to use multiple IMUs in conjunction with GPS to enhance performance and increase accuracy. In the work presented in this article, we have applied two different arrangements, a basic and a planar one. Furthermore we have calibrated three low-cost IMUs to eliminate the deterministic errors. In the planar arrangement, we have conducted a registration process to transform the sensed motion to specific coordinate systems. We have performed a comparison between calibrated fused data, raw fused data of multi-IMU and high-cost IMU. Such calibration in combination with registration and fusion has not been considered in previous work.

This article proceeds as follows. Section 2 describes the theoretical aspects of our algorithm for multi-IMU fusion. Section 3, explains the implemented hardware setup. The practical experiments are shown in section 4. The results of the experiments are presented in section 5, verifying the aim of this research. In section 6 we discuss the limitations and further research issues of our approach.

2 PIPELINE FOR MULTI-IMU CALIBRATION AND FUSION

The mathematical model for multi-IMU calibration and fusion consists of several steps (see Fig. 1). Starting with the raw data of several IMUs, we individually calibrate each IMU (section 2.1). We then describe how to register several IMUs as a joint fixed setup, arranged either in a plane or in 3D (section 2.2). Finally, we present a sensor fusion approach based on a federated Kalman filter in section 2.3. A real implementation of the system is presented in section 3. It is tested in section 4. The results are presented in section 5.

*e-mail: adnane.jadid@tum.de
†e-mail: linda.rudolph@tum.de
‡e-mail: pankratz@in.tum.de
§e-mail: kaiii.wu@tum.de
¶e-mail: pengyuan.wang@tum.de
‖e-mail: klinker@in.tum.de

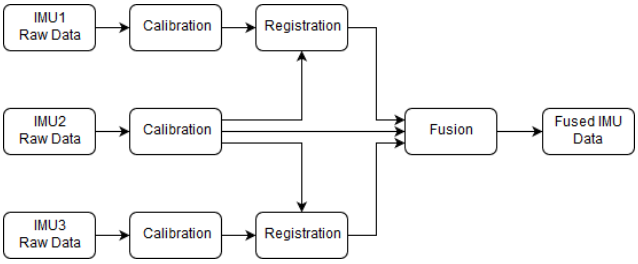

Figure 1: Experimental Process

2.1 Calibration of a Single IMU

The accuracy of an IMU depends on a variety of errors and on the effectiveness of the updating procedure in reducing these errors. When integrating linear accelerations and angular rates to calculate the position and orientation of an object, measurement errors are accumulated. They cause the so-called drift error, which is a major disadvantage of IMUs. Thus, it is of essential importance that errors be kept to a minimum.

The sensor errors of the gyroscopes and the accelerometers can be divided into a deterministic (constant) part and a stochastic (random) part. The deterministic part includes a bias (offset), an axis misalignment and a scale factor. These can be determined by calibration and can therefore be removed from the raw measurements (see Sections 2.1.1 and 2.1.2). The random part includes, for example, bias drift, and random noise (see Section 2.1.3). These errors need to be sampled during the calibration process such that they can be described in a stochastic model and included as a filter in the sensor fusion process (e.g., in the Kalman filter state vector [6]) (see Section 2.3).

There are various methods to calibrate IMUs. In this study, we used the calibration technique from Tedaldi et al. which does not require high end equipment such as high precision rate table [16], using the error models that are described below.

2.1.1 Calibration of an Accelerometer

Due to imprecise construction, the three accelerometers of an IMU do not constitute a perfect Euclidean coordinate system. They thus do not measure acceleration in three completely uncorrelated directions. Rather, the axes are skewed. Furthermore, the measurements are scaled and they have a bias (offset). In consequence, the acceleration vector defined by the measurements of the three accelerometers at a fixed IMU pose k, $a_{s,k}$, deviates from the real physical pose vector, $a_{p,k}$.

To discount these imprecisions, we define an axis misalignment matrix, M_a, a scale factor matrix, S_a, and a bias vector vector b_a. We determine these correction parameters during the calibration process, taking a large set of measurements for each of K different IMU poses.

Eq. 1 describes the transformation of the k^{th} acceleration measurement $a_{s,k}$ back to the unskewed, unscaled and unbiased real physical vector $a_{p,k}$.

$$\begin{aligned} a_{p,k} &= M_a \cdot S_a \cdot (a_{s,k} - b_a) \\ &= E_a \cdot (a_{s,k} - b_a) \\ &= h(a_{s,k}, \theta_a) \end{aligned} \tag{1}$$

with

$$M_a = \begin{pmatrix} 1 & -\alpha_{y,z} & \alpha_{z,y} \\ 0 & 1 & -\alpha_{z,x} \\ 0 & 0 & 1 \end{pmatrix}, \quad S_a = \begin{pmatrix} S_{a_x} & 0 & 0 \\ 0 & S_{a_y} & 0 \\ 0 & 0 & S_{a_z} \end{pmatrix},$$

$$E_a = M_a \cdot S_a = \begin{pmatrix} e_{0,0} & e_{0,1} & e_{0,2} \\ 0 & e_{1,1} & e_{1,2} \\ 0 & 0 & e_{2,2} \end{pmatrix}, \quad \text{and } b_a = \begin{pmatrix} b_{a_x} \\ b_{a_y} \\ b_{a_z} \end{pmatrix}.$$

To calibrate the accelerometer, we define the cost function $L(\theta_a)$ (Eq. 2). For a static (no motion) setup at IMU pose k, it relates the corrected accelerometer vectors $h(a_{s,k}, \theta_a)$ to the gravity vector, g.

$$L(\theta_a) = \sum_{k=0}^{K-1} (\|g\|^2 - \|h(a_{s,k}, \theta_a)\|^2)^2 \tag{2}$$

$\theta_a = \{e_{0,0}, e_{0,1}, e_{0,2}, e_{1,1}, e_{1,2}, e_{2,2}, b_{a_x}, b_{a_y}, b_{a_z}\}$ defines the vector of nine unknown parameters. $\|g\|$ is the magnitude of the local gravity vector.

The cost function can be optimized by applying the *Levenberg-Marquardt* algorithm over $K \geq 9$ sets of static (no motion) measurements.

2.1.2 Calibration of a Gyroscope

Similarly, Eq. 3 gives the error model for the gyroscope. Let $\omega_{s,k}$ be the k^{th} angular velocity vector measured by the gyroscope, and $\omega_{p,k}$ the corresponding unskewed, unscaled and unbiased physical vector of the angular velocity. We define an axis misalignment matrix, M_ω, a scale factor matrix, S_ω, and a bias vector vector b_ω.

$$\begin{aligned} \omega_{p,k} &= M_\omega \cdot S_\omega \cdot (\omega_{s,k} - b_\omega) \\ &= F_\omega \cdot (\omega_{s,k} - b_\omega) \end{aligned} \tag{3}$$

with

$$M_\omega = \begin{pmatrix} 1 & -\beta_{y,z} & \beta_{z,x} \\ \beta_{x,z} & 1 & -\beta_{z,x} \\ -\beta_{x,y} & \beta_{y,x} & 1 \end{pmatrix}, \quad S_\omega = \begin{pmatrix} S_{\omega_x} & 0 & 0 \\ 0 & S_{\omega_y} & 0 \\ 0 & 0 & S_{\omega_z} \end{pmatrix},$$

$$F_\omega = M_\omega \cdot S_\omega = \begin{pmatrix} f_{0,0} & f_{0,1} & f_{0,2} \\ f_{1,0} & f_{1,1} & f_{1,2} \\ f_{2,0} & f_{2,1} & f_{2,2} \end{pmatrix}, \quad \text{and } b_\omega = \begin{pmatrix} b_{\omega_x} \\ b_{\omega_y} \\ b_{\omega_z} \end{pmatrix}.$$

The bias vector b_ω can be calculated by averaging the static measurements of the gyroscope.

To calibrate the gyroscope, we define the cost function $L(\theta_\omega)$ (Eq. 4). It relates the the k^{th} gravity versor, measured by the calibrated accelerometer in the k^{th} static measurement $u_{a,k}$, to a versor $u_{\omega,k}$ that is given by function Ψ in Eq 5 as described below.

$$L(\theta_\omega) = \sum_{k=1}^{K-1} \|u_{a,k} - u_{\omega,k}\|^2 \tag{4}$$

$$u_{\omega,k} = \Psi(\omega_{s,k}, u_{a,k-1}) \tag{5}$$

Ψ calculates the current versor $u_{\omega,k}$ by integrating from the previous $k-1^{th}$ gravity versor (as measured by the calibrated accelerometer $u_{a,k-1}$) the current versor $u_{\omega,k}$ based on $\omega_{s,k}$, the angular velocity sensed during the rotation movements between the $k-1^{th}$ and the k^{th} static measurements. $\omega_{s,k}$ is integrated to get the orientation (quaternion), which can be multiplied with $u_{a,k-1}$ to calculate $u_{\omega,k}$.

$\theta_\omega = \{f_{0,0}, f_{0,1}, f_{0,2}, f_{1,0}, f_{1,1}, f_{1,2}, f_{2,0}, f_{2,1}, f_{2,2}\}$ defines a vector of nine unknown parameters. These can be determined by minimizing the cost function (see Eq. 4) with the *Levenberg-Marquardt* algorithm.

The calibration procedure collects K sets of static measurements and K-1 sets of rotation measurements between the static measurements.

2.1.3 Allan Variance

The random part of the sensor errors of accelerometers and gyroscopes concerns issues such as bias drift, and random noise. Bias drift, or bias instability, is caused by random flickering of

the electronics to fluctuate unpredictably. Another issue is quantization noise, as well as angle/velocity random walk noise and rate/acceleration walk noise.

Allan variance (AV) [8] is a method to address these issues. It is used to characterise various types of noise terms in the inertial sensor data [4]. It divides a given input signal $w(t)$ into a set of $k \in \{0 \dots K-1\}$ local windows (overlapping or not) of width τ, calculating the average $\bar{w}(t,\tau)_k$ for each window k. It then computes the squared difference $(\bar{w}(t,\tau)_k - \bar{w}(t,\tau)_{k-1})^2$ between neighboring averages and determines the mean squared difference across all windows $k \in \{0 \dots K-1\}$. This can be expressed for varying window sizes as a function of τ (see Eq. 6).

$$\sigma^2(\tau) = \frac{1}{K} \sum_{k=0}^{K-1} (\bar{w}(t,\tau)_k - \bar{w}(t,\tau)_{k-1})^2 \tag{6}$$

$\sigma^2(\tau)$ describes the root mean square random drift error as a function of averaging time τ. It has the expressive power to describe noise with respect to different frequencies (window sizes). It is a characteristic curve whose inspection provides systematic characterisation of various random errors present in the inertial sensor output data [9, 13, 18]. Fig 2 is a sample log-log plot of $\sigma(\tau)$ versus τ.

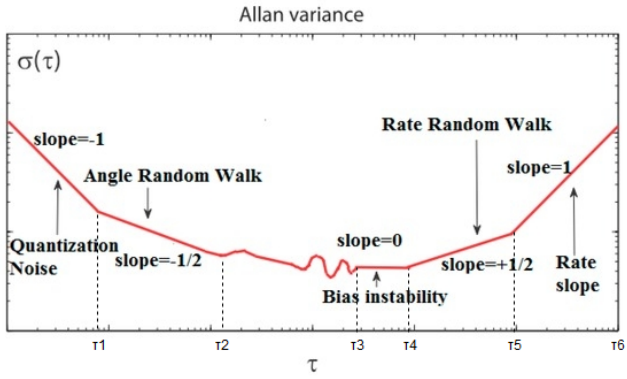

Figure 2: Sample Allan variance plot for gyroscope (adapted from [18])

This allows easy identification of various random processes that exist in the data. They can be determined based on the local slope of the function, yielding five ranges. Each range is associated with different physical sensing issues: quantization noise, angle random walk (velocity random walk, resp.), bias instability, rate random walk (acceleration random walk, resp.) and rate slope.

$$\sigma^2(\tau) = \begin{cases} \sigma_Q(\tau) & \text{if } 0 \le \tau \le \tau_1; \text{ slope } = -1 \\ \sigma_{ARW}(\tau) & \text{if } \tau_1 \le \tau \le \tau_2; \text{ slope } = -1/2 \\ \sigma_{BI}(\tau) & \text{if } \tau_3 \le \tau \le \tau_4; \text{ slope } = 0 \\ \sigma_{RRW}(\tau) & \text{if } \tau_4 \le \tau \le \tau_5; \text{ slope } = 1/2 \\ \sigma_{RS}(\tau) & \text{if } \tau_5 \le \tau \le \tau_6; \text{ slope } = 1 \end{cases} \tag{7}$$

Subsequently, we concentrate on two random errors which can be calculated by AV. Those random errors will be used by the sensor fusion in section 2.3.

Angle random walk (ARW) for gyroscopes and **Velocity random walk (VRW)** for accelerometers, respectively: High frequency noise terms, that have correlation time much shorter than the sample time can contribute to the gyro angle (or accelerometer velocity) random walk. The Allan variance for angle (velocity) random walk becomes

$$\sigma^2(\tau) = \frac{Q^2}{\tau} \tag{8}$$

$$Q = \sigma_{ARW}(\tau) \times \sqrt{\tau} \tag{9}$$

Eq 8 indicates that a log-log plot of $\sigma^2(\tau)$ has a slope of -1/2.

Rate random walk(RRW) for gyroscopes and **Acceleration random walk (ARW)** for accelerometers, respectively: This noise is a result of integrating wideband acceleration PSD. This is a random process of uncertain origin, possibly a limiting case of an exponentially correlated noise with a very long correlation time. The Allan variance of rate random walk is

$$\sigma_{RRW}{}^2(\tau) = (\frac{K^2}{3}) \times \tau \tag{10}$$

$$K = \sigma_{RRW}(\tau) \times \sqrt{\frac{3}{\tau}} \tag{11}$$

This indicates that rate random walk is represented by a slope of + 1/2 on a log-log plot $\sigma^2(\tau)$ of versus τ.

2.2 Arrangement and Registration of Several IMUs

2.2.1 Spatial Arrangement

With six degrees for freedom (DoF) per IMU, a large number of potential arrangements exist for aligning the IMUs with respect to position and/or orientation (18 DoF in total). We intend to investigate whether partial alignments help obtaining more accurate results or whether it is better to vary over as many degrees of freedom as possible.

We begin with the most basic arrangement, placing the three IMUs in a row with aligned orientations for the *x*-, *y*- and *z*-axes (see Fig. 3a). Mathematically, the change in positions does not have an impact on the measurements. Thus, in principle, this arrangement yields a test situation to fuse identical measurements from 3 IMUs. The main coordinate system belongs to the middle IMU.

In a second setup, we position the IMUs in a planar arrangement, keeping the same orientation for the *x*-axis, but rotating the arrangement by 90° and 180° around the *x*-axis and thereby shuffling the orientations of the *y*- and *z*-axes. The coordinate system of the IMU in the front side is choosen as the main coordinate system.

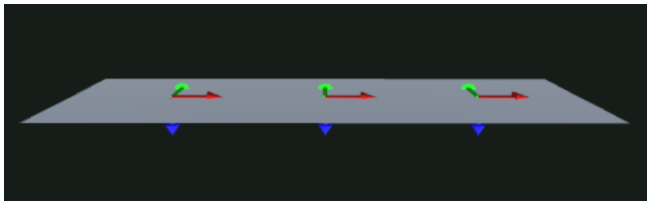

a) Linear placement, aligned orientations of the x-, y- and z-axes

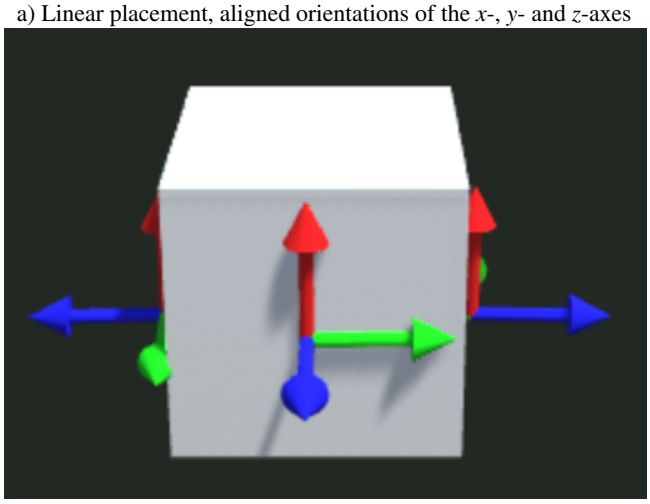

b) Planar placement, aligned orientation $\vec{x}$, rotated orientations for the y- and z-axes

Figure 3: Two conceptual arrangements of 3 IMUs

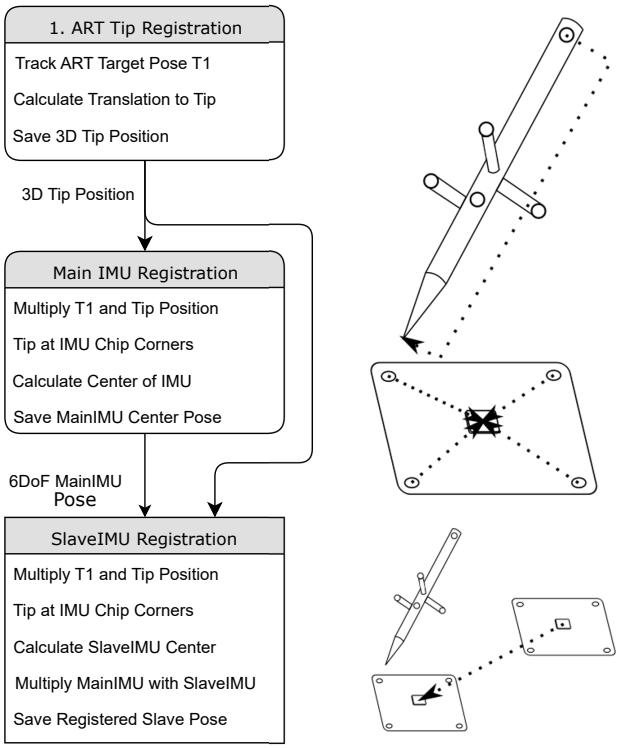

Figure 4: Registration of slave-IMU to Main-IMU

Figure 4 shows the registration process. For the registration an outside-in optical tracking system (ART) is used [1]. We begin by registering the tip of a pointer target in the optical tracking system [17]. With this pointer we then determine the pose of the main IMU in the ART tracking coordinate system by tipping on the four corners of its circuit board. The body coordinate system of each IMU is in the centre of the circuit board. Similar to the main IMU, we calculate the pose of the slave IMUs. Each of these poses can be registered with respect to the main IMU by inverting the pose of the main IMU and multiplying with the pose of the respective slave IMU (see Fig. 5 [12].

2.2.2 Registration

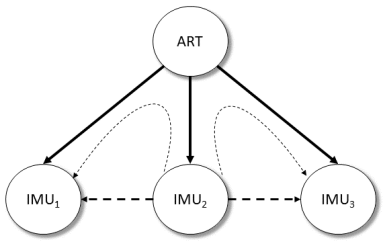

Figure 5: Spatial relationships between the IMUs and the outside-in cameras system needed for registration

Each IMU sensor measures the motion in its own body coordinate system. Since the three IMUs are rigidly attached, they exert the same motion. The acceleration and the angular velocity of the all IMUs can be transformed to the main coordinate system when the transformations $R|T$ between the main IMU and the two slave IMUs are known, i.e., when the coordinate systems are registered to the main IMU. The translation component cancels out because acceleration is a vector. Thus, only the rotation transformations need to be determined.

2.3 Sensor Fusion

2.3.1 Principle of Decentralised Filtering

To fuse the tracking data from three IMUs, we use decentralised filtering. It is a two-stage data processing technique. In the first

stage, each local processor uses its own data to make a best local estimate. In the second stage, these estimates are combined across all local sensors. The local estimates are fused by a master filter to make a best global estimate of the state vector of the entire system.

Federated Kalman filtering is a decentralised filtering algorithm with a two-level structure as shown in Fig 6. The difference between the federated Kalman filter and other decentralised filters is that the federated Kalman filter contains an information sharing process. During this process, the total system information is divided among the local filters based on an information sharing principle. The basic concepts of information sharing also include that it can perform local time propagation and measurement update processing (adding local sensor information) and it can recombine the updated local information into a new total sum [3, 7, 19].

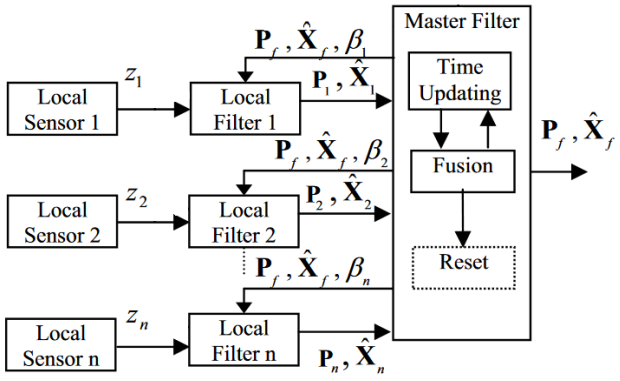

Figure 6: Federated Kalman filtering architecture (adapted from [19])

The steps involved in the decentralised filtering process will now be described in detail.

2.3.2 Local Filters

For each local filter $i = 1,2,3$, we use an Unscented Kalman Filter (UKF) for the triaxial accelerometer bundles and for the triaxial gyroscope bundles.

The motion model the accelerometers of IMU_i, $i = 1,2,3$ consists of 1) the estimated state vector $\hat{X}_i$ defined by position p_i, velocity v_i and acceleration a_i, 2) the observation vector z_i defined by measured acceleration a_i, 3) the transition matrix F_i for the prediction step assuming constant acceleration, 4) the observation model H_i, 5) the process noise Q_i: a 3x3 white noise matrix (VRW), 6) the measurement noise R_i: a 1x1 matrix (RRW) and 7) the state variance matrix P_i: a 3x3 matrix

with

$$\hat{X}_i = \begin{bmatrix} p_i \\ v_i \\ a_i \end{bmatrix}, \quad z_i = \begin{bmatrix} a_i \end{bmatrix}, \quad F_i = \begin{bmatrix} 1 & \Delta t & 0.5\Delta t^2 \\ 0 & 1 & \Delta t \\ 0 & 0 & 1 \end{bmatrix}, \quad H_i = \begin{bmatrix} 0 & 0 & 1 \end{bmatrix}$$

Similarly, the motion model of the three gyroscopes IMU_i $i = 1,2,3$ consists of 1) the estimated state vector $\hat{X}_i$ defined by angle α_i and angular velocity ω_i, 2) the observation vector z_i defined by measured angular velocity ω_i, 3) the transition matrix F_i for prediction step, assuming constant angular velocity, 4) the observation model H_i, 5) the process noise Q_i: a 3x3 white noise matrix (ARW), 6) the measurement noise R_i: a 1x1 matrix (RRW) and 7) the state variance matrix P_i: a 3x3 matrix

with

$$\hat{X}_i = \begin{bmatrix} \alpha_i \\ \omega_i \end{bmatrix}, \quad z_i = \begin{bmatrix} \omega_i \end{bmatrix}, \quad F_i = \begin{bmatrix} 1 & \Delta t \\ 0 & 1 \end{bmatrix}, \quad H_i = \begin{bmatrix} 0 & 1 \end{bmatrix}$$

Each local filter $i = 1,2,3$ receives as input the observation vector z_i from the local sensor i, consisting of acceleration data a_i and angular velocity ω_i. As output, they each provide their updated state vector $\hat{X}_i$ as well as their state variance matrix P_i

2.3.3 Master Filter

The master filter is also an Unscented Kalman Filter (UKF). It receives the outputs $\hat{x}_i$, P_i from all local filters $i = 1,2,3$ as input. It generates as outputs the updated state vector of the overall system state $\hat{X}_f$, as well as an overall state variance estimate P_f and a scalar weight β_i . These are fed back to all local filters to serve as additional inputs, influencing their states and their noise estimates. Furthermore, they constitute the overall system output, made available to applications using the IMUs as a bundled tracking device.

Internally, the master filter takes the system states and the state variance matrices of the local filters and performs the following steps:

1. **Time Update:** compute a time update of $\hat{X}_f$, P_f
$$X_m = F \cdot X_f,$$
$$P_m = F \cdot P_f \cdot F^T + Q$$
2. **Fusion:** compute P_f, $\hat{X}_f$ and β_i
$$P_f^{-1} = P_m^{-1} + \sum_{i=1}^{n} P_i^{-1}$$
$$\hat{X}_f = P_m^{-1} \cdot X_m + \sum_{i=1}^{n} P_i^{-1} \cdot \hat{X}_i$$
let Λ_i be the eigenvalue of $P_i.P_i^T$
$$\beta_i = \frac{tr(\Lambda_i)}{tr(\Lambda_m) + \sum_{i=1}^{n} tr(\Lambda_i)}$$
3. **Updating local value:** update $\hat{X}_i$, P_i according to $\widehat{X}_f$, P_f
$$\hat{X}_i = \hat{X}_f,$$
$$P_i = \beta_i^{-1} \cdot P_f$$

3 Implementation of Multi-IMU Setups

One of our assumptions is, that there is a difference in the fusion quality between rectified and not rectified Multi-IMU Setups. To verify this hypothesis, we have built a nearly rectified linear IMU setup on a breadboard (see 7 a) and a not rectified IMU setup, where the IMUs are attached to three sides of a cube and the coordinate systems thus have different orientations. The cube-based setup imitates the conceptional arrangement of Figure 3 b) with a deviation of 14%, due to the usage of a styrofoam cube. Because of this deviation, it was necessary to execute the registration step of section 2.2.2 and not use the conceptual rotation matrices between the IMU coordinate systems for registration purpose.

Our installation is based on an Arduino [2] platform. It is a low-cost electronic platform that has interchangeable easy-to-use hardware and software. For both setups, we use an Arduino Mega 2560 as a programmable microcontroller. We use the I2C protocol to collect the data of three IMU sensors. The three IMUs are connected via the TCA9548A I2C multiplexer to the microcontroller.

The setup on the breadboard (see Fig 7a) consists of three different IMUs (DFRobot SEN0140, Adafruit BNO55, Waveshare MPU9255), a multiplexer and a microcontroller. The setup on the cube (see Fig 7b) consists of three equivalent Adefruit BNO55 IMUs, a multiplexer and a microcontroller.

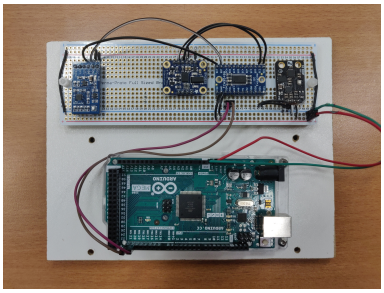

a) Arrangement on a breadboard

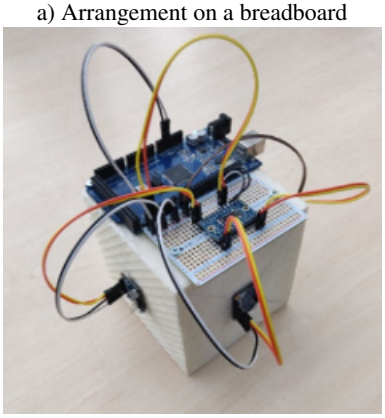

b) Arrangement on a cube

Figure 7: Realized arrangements of three IMUs.

The hardware is connected via *A to B USB cabling* to a computer containing the Arduino 1.8.8 software for uploading data. Data were processed in the Arduino onboard system and output through serial connection for analysis and results. Coolterm 1.5.0 was used to save the serial data.

4 Test Procedures

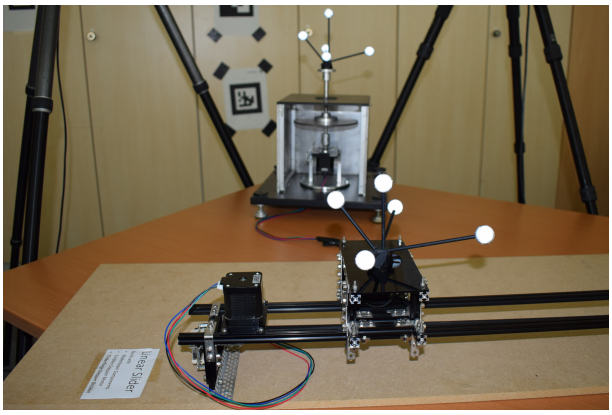

Figure 8: Setup Configurations for Physical Stepper Motors. The linear slider is shown in front and the rotation table in background.

The purpose of the article is to compare the quality of the suggested fusion against a single high-cost IMU. Therefore, a highly dynamic setup for the one-dimensional movement was built. This setup consists of a linear slider and a rotation platform, both driven by similar stepper motors. The Osmtec Nema 17 stepper motors [11] have a step angle of 1.8 ° and a torque of 0.43 Nm. The conversion factor between the rotational movement of the stepper motor and the toothed belt drove linear movement of the slider was measured with an ART Tracking System [1] and is shown in Equation 12.

$$1\,\mathrm{st} \approxeq 0.0249\,\mathrm{m} \tag{12}$$

With a Tinkerforge Stepper Brick [10], we are able to control the driven steps, as well as the velocity, acceleration and deceleration. Afterwards, we calculate motion models for the linear and angular motion. These motion models have four phases: constant acceleration, constant velocity, constant deceleration and stop. Each phase should be at least four times as long as the lowest frequency of the IMUs to avoid sampling inaccuracies. Furthermore, especially for the accelerometer, it was necessary to find an acceleration value, that is higher than the noise band. With this parameters, the motion model shown in figure Figure 9 was calculated.

Fewer iterations would have produced less statistical meaningfulness, more iterations would have provoked heating of the stepper motor, what would have been a new source of error. All measurements were taken in the evening to avoid system shocks, triggered by walkers-by in the vicinity. For comparison purpose, the same measurements were taken with the XSENS MTi-3-8A7G6 as a representative of high-cost IMUs.

5 Error Calculation and Results

The evaluation of our pipeline bases on a comparison with several intermediate results, the high-cost IMU and.

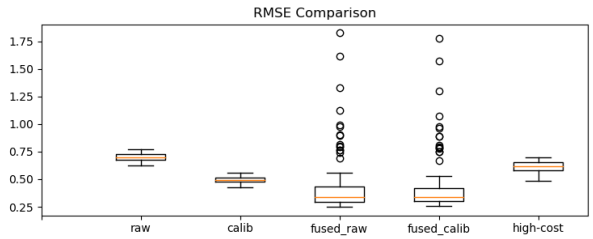

a) The accelerometer measurements of the cubical sensor setup.

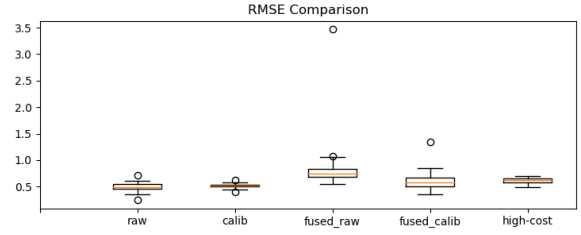

b) The accelerometer measurements of the planar sensor setup.

Figure 10: Comparision of RMSE for the accelerometer.

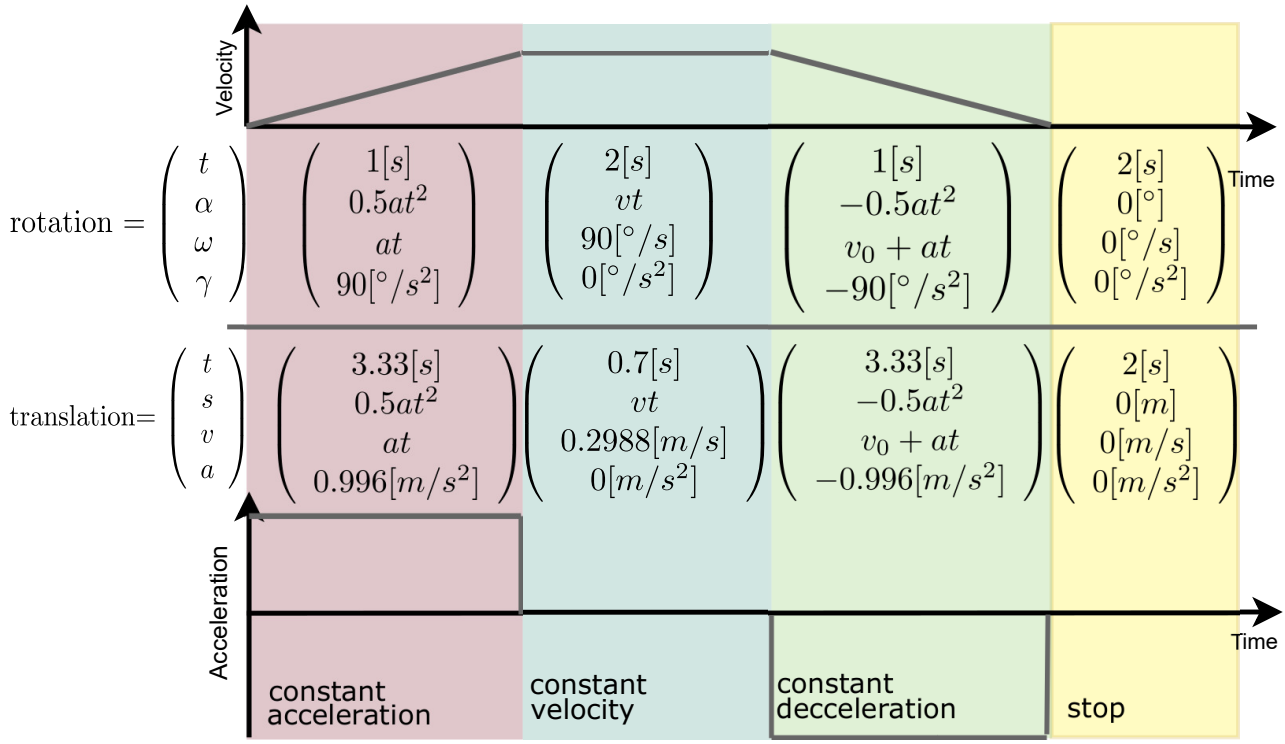

Figure 9: Dynamic evaluation motion model. α is the moved angular on the rotation platform, ω the angular velocity, γ the angular acceleration, s means the linear way on the slider, v is the linear movement and a the linear acceleration.

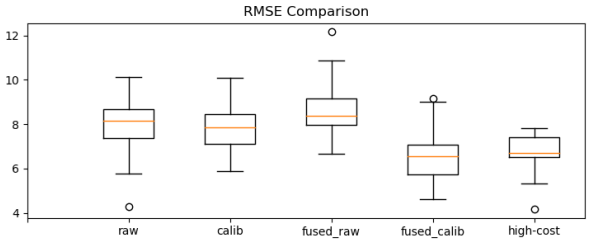

a) The gyroscope measurements of the cubical sensor setup.

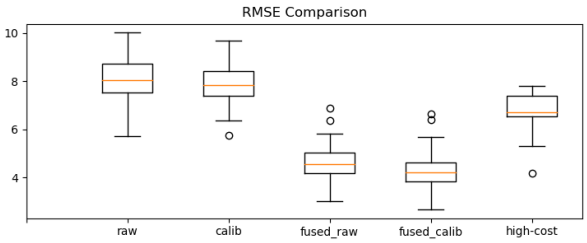

b) The gyroscope measurements of the planar sensor setup.

Figure 11: Comparision of RMSE for the gyroscope.

5.1 Error Calculation

For our motor, we assume an evenly accelerated movement such that we can use Equation 13 to calculate the motion model. Since this simplification was used for all measurements, it should change only the absolute error values, but not their interrelations.

$$s = 0.5at^2 + vt + s_0 \tag{13}$$

The measured time series were evaluated against the motion model calculating a root mean square error (RMSE see Equation 14). x represents the motion model value at time t_0 and $\hat{x}$ is the measured value at time t_0. T is the number of measurements.

$$\varepsilon = \sqrt{\sum (x - \hat{x})^2 / T} \tag{14}$$

For comparison purpose the following measurements and parameter combinations were regarded:

1. **Raw** Calculates the RMSE between the raw sensor data and the motion model for a single low-cost IMU.
2. **Calibrated** Calculates the RMSE between a single calibrated low-cost IMU and the motion model.
3. **Fused Raw** RMSE of three fused raw low-cost IMU measurements without calibration and the motion model.
4. **Fused Calib** RMSE of three fused calibrated low-cost IMU measurements and the motion model.
5. **High-Cost** RMSE of a single high-cost IMU and the motion model.

These combinations were evaluated for both motion models (slider and rotation platform) and both Multi-IMU setups (linear and cubical setup).

5.2 Results

Table 1 shows the mean RMSE values for each 80 iteration measurement series and the Figures 10 and 11 show box-plots, that shows the statistical spread of the results. What our results clearly show is, that three low-cost calibrated and fused IMUs can produce as accurate results as one high-cost IMU. The calibration step always increases the precision of the results, while the fusion step produces

some outliers, and so mitigates the precision. Uncalibrated fused IMUs produce sometimes (see Figure 10 and 11) worse results then single low-cost uncalibrated IMUs. This effect appears, when one of the three fused IMUs sends notably worse data than the others. For example, in the measurements shown in Figure 10, the main IMU has a Mean Raw Data RMSE of $0.6978 m/s^2$, but the second slave IMU has a Mean Raw Data RMSE of $2.0958 m/s^2$. The negative effect disappears when the IMUs were calibrated before fusion. For now, we can not make a clear statement, whether it is better to use a plate or a cube setup.

		rotation		slider	
single	raw	$7.9871 \frac{°}{s}$		$0.6978 \frac{m}{s^2}$	
	calibrated	$7.8708 \frac{°}{s}$		$0.4951 \frac{m}{s^2}$	
		plate	cube	plate	cube
fused	raw	$4.6392 \frac{°}{s}$	$8.6335 \frac{°}{s}$	$0.7962 \frac{m}{s^2}$	$0.4603 \frac{m}{s^2}$
	calibrated	$4.2951 \frac{°}{s}$	$6.5493 \frac{°}{s}$	$0.5901 \frac{m}{s^2}$	$0.4559 \frac{m}{s^2}$
	high-cost	$6.7723 \frac{°}{s}$		$0.6177 \frac{m}{s^2}$	

Table 1: RMSE values for all configurations

6 Limitation and Future Work

As every physical evaluation method, our dynamic measurement model does not work ideal. In this chapter, we discuss the most influential limitations of our measurements and how to overcome them in future experiments.

6.1 Limitation

6.1.1 Setup assembling limitations

After the cubical setup is built with a styrofoam core, the screws of the IMUs have a scope and can have changed their position while the experiments. In follow-up investigations, we plan to use a harder material like acrylic or 3D printing filaments as the core of our setups. A second, more important issue is, that we have used three Adafruit IMUs for the cubical setup, but three not identical IMUs from different manufacturers for the linear setup. Unfortunately, in the linear case, the quality differences of the low-cost IMUs have such an impact, that we can't verify our hypothesis about the significantly different results based on different shapes without regarding this issue. So in our next experiments, identical and not identical setups have to be regarded separately.

6.1.2 Error in Step-Motor

According to [11], the used Step-Motor has a location error of $\pm 5\%$. Actually, we have no possibilities to overcome this mistake. Also, we have to admit, that it is not physically accurate to assume an evenly accelerated movement, but as said in Chapter 5, since this simplification was used for all measurements, it should change only the absolute error values, but not their interrelations.

6.1.3 Perturbation during the test

IMUs are very prone to shocks. So if somebody acts near to the setup, the shocks were registered by the IMUs and distort the results. Our first action against this issue was to measure in the evening when fewer persons are in the lab. For future measurements, we also intend to use a remote measurement system in a locked room between 3 and 5 am to avoid distortions triggered by the experimenter or the metro. Also, especially the linear slider generates vibrations because of friction, what influences the Acceleration Measurements and can be one factor, why we only have meaningful results for the gyroscope.

6.2 Future Work

6.2.1 Sensor Data Synchronisation

Imu's data was collected and fused offline.Therefor an investigation of the realtime multi-IMU sensor fusion approach is recommended and will be following. Hardware or software synchronisation is essential for a realtime sensor fusion.

6.2.2 Visual and Inertial Sensor Fusion

Another interesting study is the fusion of visual and inertial sensors. We will combine multi-IMU with a target tracked by the visual sensors in Outside-in scenario. we will also study the impact of multi-imu combination with visual sensors in Inside-out approach.

6.2.3 Optimal Number of IMUs

Our setups consist of three IMUs. But for now, we have no evidence, whether this is the optimal amount or not. In the future, it should be investigated which amount of IMUs promises the highest quality improvement. If we find a point of inflection in the dependency between the amount of IMUs and quality improvement, it is possible to optimize our system.

6.2.4 Orientation of the IMUs

For now, we have tested only one non-linear MultiIMU Setup with rotations of nearly 90° it was not possible for this article to distinguish the impact of this orientations from the impact of using identical and different IMUs it could be helpful to analyze a variety of setups with identical IMUs, but different orientations.

7 Conclusion

For prototyping, consumer market products and self-developed research devices in the field of Mixed Reality the usage of low-cost IMUs provides new interaction and localisation possibilities. Our fusion pipeline also provides the chance to improve existing setups by adding new IMUs instead of replacing the existing sensors with higher-cost IMUs. Especially for a set of three identical low-cost IMUs, we were able to prove, that our pipeline produces results with similar or even better results than one high-cost IMU. Furthermore, we present a dynamic movement measurement system for quality evaluation, that can be used for multi-IMU as well for combined sensor setups or visual sensors.

Acknowledgments

This Work was supported by German Ministry of Education and Research (BMBF) within the project MATALPROFI (01IS17103B) and by German Federal Ministry for Economic Affairs and Energy (BMWI) within the project (AiF ZIM ZF4086002SS7).

References

[1] Advanced realtime tracking. https://ar-tracking.com/.

[2] Arduino. https://www.arduino.cc/.

[3] J. B. Bancroft and G. Lachapelle. Data Fusion Algorithms for Multiple Inertial Measurement Units. *Sensors*, 11(7):6771–6798, jun 2011. doi: 10.3390/s110706771

[4] N. El-Sheimy, H. Hou, and X. Niu. Analysis and modeling of inertial sensors using allan variance. *Instrumentation and Measurement, IEEE Transactions on*, 57:140 – 149, 02 2008. doi: 10.1109/TIM.2007.908635

[5] D. Hazry, M. Sofian, and a. Z. Azfar. Study of Inertial Measurement Unit Sensor. *International Conference on ManMachine Systems ICoMMS*, pp. 11–13, October 2009.

[6] H. Hou. *Modeling inertial sensors errors using Allan variance*. University of Calgary, Department of Geomatics Engineering, 2004.

[7] G. Hu, S. Gao, Y. Zhong, B. Gao, and A. Subic. Modified federated Kalman filter for INS/GNSS/CNS integration. *Proceedings of the Institution of Mechanical Engineers, Part G: Journal of Aerospace Engineering*, 230(1):30–44, jan 2016. doi: 10.1177/0954410015586860

[8] IEEE Aerospace and Electronic Systems Society. Gyro and Accelerometer Panel. and Institute of Electrical and Electronics Engineers. *IEEE standard specification format guide and test procedure for single-axis interferometric fiber optic gyros*. Institute of Electrical and Electronics Engineers, 1998.

[9] J. Li and J. Fang. Not Fully Overlapping Allan Variance and Total Variance for Inertial Sensor Stochastic Error Analysis. *IEEE Transactions on Instrumentation and Measurement*, 62(10):2659–2672, oct 2013. doi: 10.1109/TIM.2013.2258769

[10] B. Nordmayer. Tinkerforge Stepper Brick. "`https://www.tinkerforge.com/de/doc/Hardware/Bricks/Stepper_Brick.html#technische-spezifikation`", visited 2019-03-19.

[11] Osmtec. Nema 17. "`https://www.tinkerforge.com/de/shop/stepper-motor-nema-17-043nm.html`", visited 2019-03-19.

[12] D. Pustka, M. J. Huber, C. A. L. Waechter, F. Echtler, P. Keitler, J. Newman, D. Schmalstieg, and G. Klinker. Automatic configuration of pervasive sensor networks for augmented reality. *IEEE Pervasive Computing*, 10(3):68–79, 2011.

[13] R. Ramalingam, G. Anitha, and J. Shanmugam. Microelectromechnical Systems Inertial Measurement Unit Error Modelling and Error Analysis for Low-cost Strapdown Inertial Navigation System. *Defence Science Journal*, 59(6):650–658, nov 2009. doi: 10.14429/dsj.59.1571

[14] A. M. Shahri and R. Rasoulzadeh. Implementation of a Low- Cost Multi- IMU by Using Information Form of a Steady State Kalman Filter. *AUT Journal of Electrical Engineering*, 49(2):195–204, dec 2017. doi: 10.22060/EEJ.2017.12045.5028

[15] I. Skog, J. O. Nilsson, and P. Handel. An open-source multi inertial measurement unit (MIMU) platform. In *1st IEEE International Symposium on Inertial Sensors and Systems, ISISS 2014 - Proceedings*, 2014. doi: 10.1109/ISISS.2014.6782523

[16] D. Tedaldi, A. Pretto, and E. Menegatti. A robust and easy to implement method for IMU calibration without external equipments. In *2014 IEEE International Conference on Robotics and Automation (ICRA)*, pp. 3042–3049. IEEE, may 2014. doi: 10.1109/ICRA.2014.6907297

[17] M. Tuceryan, D. S. Greer, and R. T. Whitaker. Calibration Requirements and Procedures for a Monitor-Based Augmented Reality System. *IEEE Transactions on Visualization and Computer Graphics*, 1(3):255–273, 1995.

[18] L. Wang, C. Zhang, S. Gao, T. Wang, T. Lin, and X. Li. Application of fast dynamic allan variance for the characterization of fogs-based measurement while drilling. *Sensors*, 16(12), 2016. doi: 10.3390/s16122078

[19] H. Zhang, B. Lennox, P. R. Goulding, and Y. Wang. Adaptive Information Sharing Factors In Federated Kalman Filtering. *IFAC Proceedings Volumes*, 35(1):79–84, jan 2002. doi: 10.3182/20020721-6-ES-1901.00666